Sound & Vibration 2025, 59(3), 2973.
https://doi.org/10.59400/sv2973

Article

Optimization of noise barriers in a ±500 kV switchyard: Field testing and numerical modelling

Li Li[1], Shenghui Xu[2], Xing Du[3,*], Cai Zeng[3], Meng Wei[1], Xinbiao Xiao[2]

[1] Electric Power Research Institute, Guangdong Power Grid Co., Ltd., Guangzhou, Guangdong, 510000, China
[2] State Key Laboratory of Rail Transit Vehicle System, Southwest Jiaotong University, Chengdu, Sichuan, 610031, China
[3] School of Electrical Engineering, Southwest Jiaotong University, Chengdu, Sichuan, 610031, China
*** Corresponding author:** Xing Du, duxing@swjtu.edu.cn

CITATION

Li L, Xu S, Du X, et al. Optimization of noise barriers in a ±500 kV switchyard: Field testing and numerical modelling. Sound & Vibration. 2025; 59(3): 2973. https://doi.org/10.59400/sv2973

ARTICLE INFO

Received: 19 March 2025
Accepted: 21 May 2025
Available online: 7 July 2025

Abstract: This study investigates noise characteristics of a ±500 kV high-voltage (HV) switchyard through field testing. Noise levels and spectral properties near the reactor and fence were analyzed. An acoustic boundary element method (BEM) model was developed to predict the reactor-generated noise. Using this model, the effects of fence height, the height and placement of an additional noise barrier on the combined noise reduction effects (NRE) were systematically examined. To further enhance the NRE, various top structures and sound-absorbing materials were applied to noise barriers, and their additional NREs were compared. The results indicate that increasing fence height by 1–2 m reduces the sound pressure levels (SPL) outside the fence by 1–5.8 dB. Adding L-type or T-type top structures further reduces SPLs by 0.4–4.6 dB. Installing an additional erect noise barrier between the reactor and fence reduces SPLs by 1.4–8.8 dB, with the insertion loss (IL) increasing by 0.6–2.8 dB per 1-m barrier height increase. The T-type or Y-type top structures on the barriers also reduce SPLs by 0.4–4.6 dB, while traditional sound-absorbing materials have minimal impact on the NRE.

Keywords: switchyard noise control; noise barrier; top structure; sound-absorbing materials; boundary element method

1. Introduction

The rapid growth of the national economy has driven a dramatic surge in urban electricity demand. In recent decades, urban expansion and power grid modernization have necessitated the construction of distribution substations near, or even within, residential areas [1]. The noise generated by power facilities significantly affects the physical and mental health of residents [2–5], leading to an increasing number of community complaints and legal disputes [6]. The noise of distribution substations is primarily characterized by the mid-to-low frequency components below 1000 Hz, particularly the high-order harmonic noise with a 50 Hz fundamental frequency [7–9]. Although less perceptible than high-frequency noise, low-frequency noise poses substantial health risks. Prolonged exposure to low-frequency noise may induce emotional agitation, neurasthenia, and insomnia and could potentially impact fetal development. When the SPL exceeds 60 dB(A), individuals typically experience discomfort, and in severe cases, symptoms such as tachycardia, hypertension, and restlessness [10–13]. These findings underscore the critical need for effective low-frequency noise control in substation design.

Previous studies have investigated noise prediction methodologies and various mitigation measures [14–19]. Di et al. [20] recorded the noise of substations with the voltage level of 110–1000 kV and suggested the control indices of noise at the boundary

of substations, as well as the limits of sound pressure level of octave bands. Oliveira et al. conducted a comprehensive study on the acoustic fields near urban high-voltage substations. They proposed strategies to mitigate noise pollution, such as eliminating tonal components and installing acoustic barriers [21]. Sun et al. developed an acoustic model based on transformer point sources, validated through field measurements [22]. Ruan et al. proposed an outdoor noise coherence prediction model for engineering applications, which was used to predict the coherent sound field around a substation transformer and compared with ISO 9613-12 algorithms, BEM simulations, and empirical data [23]. Gao et al. analyzed the frequency characteristics and propagation patterns of substation equipment noise using field test data, subsequently proposing optimized design schemes and control measures [24]. Wang et al. reviewed substation noise control technologies from source, propagation path, and receiver perspectives and evaluated their practical engineering applications [25]. Shi et al. introduced a noise control optimization method for main transformers based on annoyance improvement metrics, comparing different barrier configurations [26]. Wang et al. designed a natural ventilation window with coiled-up, coupled-tube silencers that effectively reduces transformer noise at key frequencies (100–500 Hz), and experiments validated the design's feasibility [27]. Zhao et al. proposed a sound field control barrier using optimized acoustic metamaterial units to reduce transformer noise by up to 25 dB at frequencies like 100 Hz and its harmonics, with a thickness of only 4 cm and ventilation [16]. Common solutions include underground transformer relocation, low-noise equipment development, transformer enclosures, and noise barriers [28–30]. However, the first two options involve lengthy implementation cycles and high costs, while enclosures impose strict requirements for ventilation, heat dissipation, and fire safety. Consequently, noise barriers have become the preferred choice for urban planners, grid operators, and environmental engineers.

Noise barriers represent one of the most widely adopted and effective noise control measures, attenuating noise during propagation. The NRE of traditional erect barriers primarily depends on height. While increasing barrier height is a common strategy to enhance the NRE, this approach elevates construction and maintenance costs and may compromise safety by obstructing operator visibility [31]. Additionally, low-frequency noise readily diffracts over barrier tops, generating secondary acoustic sources that reduce attenuation effectiveness for mid-to-low frequencies. Enhancing the NRE without increasing barrier height has emerged as a critical research priority. Optimizing geometric configurations is widely regarded as the most viable approach to improving barrier performance. Murata et al. tested Y-shaped top structures and found that adding a Y-shaped extension to a 3 m-high vertical barrier achieved an incremental 2–3 dB(A) NRE without height increase [32]. May et al. conducted field trials that demonstrated that T-shaped barriers provided 1–1.5 dB(A) higher IL than equivalent-height erect barriers [33]. Yin et al. designed an interference device based on the principle of interference noise reduction, experimentally verifying 2–3.2 dB(A) additional NREs compared to conventional barriers [34]. Veloso et al. used the Method of Fundamental Solutions (MFS) to predict the acoustic performance of sonic crystal noise barriers coated with porous concrete. The numerical models were validated experimentally and compared with finite element method (FEM) results, showing that porous concrete can enhance noise attenuation at specific frequencies [35]. Qin et al.

combined quadratic residue diffusers (QRD) with micro-perforated panels (MPP) to improve the IL of noise barriers. The study found that optimizing MPP parameters for impedance matching with QRD significantly enhanced noise reduction performance [36]. Tarrazó-Serrano et al. optimized an acoustic subwavelength slit barrier using FEM simulations and experimental validation to control low-frequency noise in industrial buildings. The optimized design achieved a 134% increase in sound attenuation in the 100–300 Hz range without altering the barrier's element count [37].

This study addresses noise issues at a ±500 kV switchyard in China (**Figure 1a**), where noise levels near the northeast fence exceed environmental standards (**Figure 1b**). Due to the switchyard's proximity to residential areas, it is classified as a noise-sensitive zone. The HV reactor, a primary source of noise, propagates sound unobstructed to the perimeter fence because there is no intervening equipment. Field tests were conducted to characterize noise levels both at the reactor and inside and outside the northeast fence. A validated noise prediction model was developed, using the measured data as input to simulate noise distributions. Optimized noise control strategies were proposed and evaluated to improve the NRE. Acoustic BEM analysis was employed to calculate noise distributions and barrier ILs, including the effects of top structures. BEM offers advantages in capturing geometric interactions, ground effects, and diffraction/reflection phenomena at barrier edges and top structures.

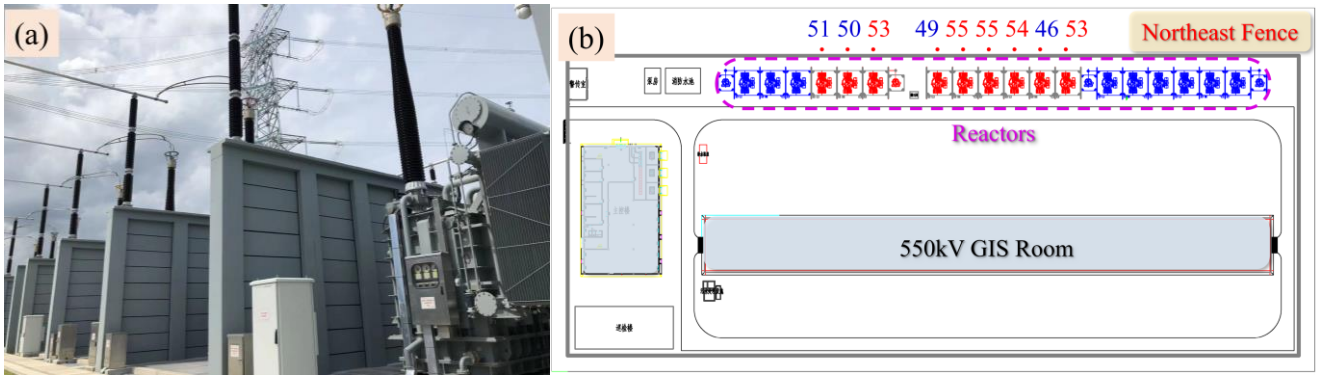

(a) **(b)**

Figure 1. ±500 kV switchyard. **(a)** HV reactor; **(b)** SPLs outside the northeast fence of the station (dBA).

2. Outdoor noise characteristics

Field tests were conducted to obtain noise data near the reactor and the station fence, offering insights into the noise levels and dominant frequencies. Noise levels were measured at various horizontal distances from the reactor and at different locations both inside and outside the station fence. **Figure 2** illustrates the layout of the acoustic measurement points (MP) and provides field photos. All MPs were positioned at a height of 1.5 m.

2.1. Noise levels

First, the noise levels in the area near the reactor and fence were analyzed. As shown in **Figure 2**, MP1–MP7 are located 1, 2, 3, 4, 5, 6, and 7 m away from the reactor, respectively, and are positioned away from the fence. MP8 is 1 m inside the

fence and approximately 6 m away from the reactor, while MP9 is 1 m outside the fence.

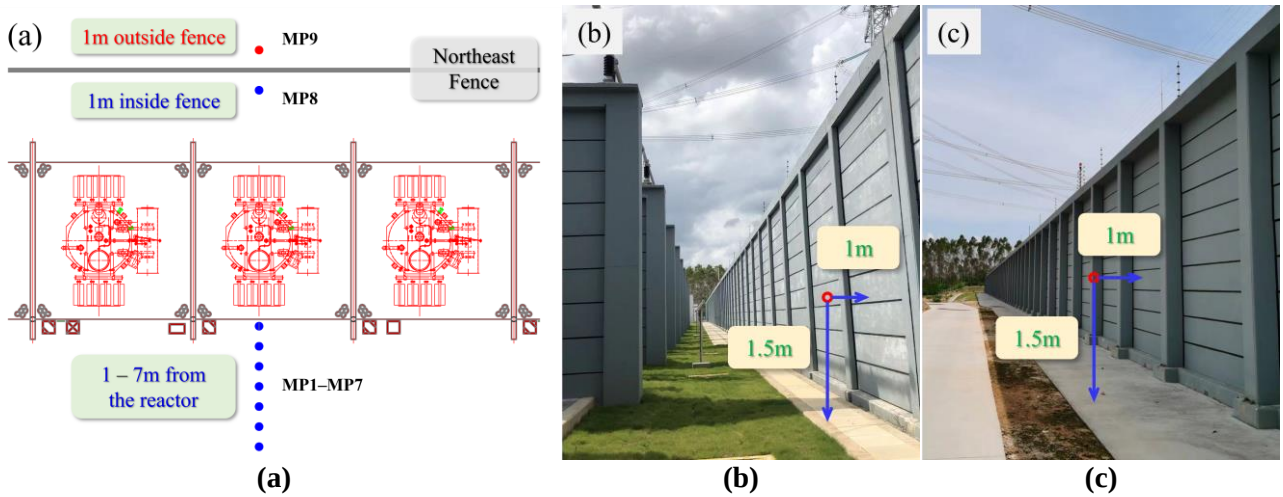

(a) **(b)** **(c)**

Figure 2. Acoustic MPs near the reactor and fence. **(a)** layout diagram; **(b)** inside the fence; **(c)** outside the fence.

Table 1 presents the noise levels at each MP. Analysis of the data in **Table 1** reveals that in the area where the reactor is farther from the fence, the noise level gradually decreases with increasing horizontal distance from the reactor. Additionally, the SPL decays more rapidly within 3 m of the reactor, decreasing by 2.6–3.1 dBA for every 1-m increase in distance. Beyond 3 m from the reactor, the noise level remains relatively stable, with an SPL range of 70.8–71.5 dBA. However, at a distance of 5 m from the reactor (MP5), the noise level significantly increases to 74 dBA, which is 3.2 dBA and 2.5 dBA higher than at MP4 and MP6, respectively. The reasons for this are as follows: first, the 5-m distance from the reactor may be influenced by radiated noise from the adjacent reactor, while areas within 5 m are shielded by the firewall and thus not affected; second, due to the standing wave effect, MP5 is located at a special position of a standing wave node, resulting in a significant increase in SPL at this location. Furthermore, the higher SPLs observed at MP6 and MP7, which are farther from the reactor, compared to those at closer MP3 and MP4, indirectly indicate that the area 5 m away from the reactor and beyond is affected by the radiated noise from the adjacent reactor.

Table 1. Noise levels near the reactor and fence (dBA).

MP. Num.	MP1	MP2	MP3	MP4	MP5	MP6	MP7	MP8	MP9
SPL	76.5	73.9	70.8	70.8	74	71.5	71.1	69.6	54.8

In the area near the fence, the noise level is relatively lower than in the area on the side of the reactor farther from the fence. The SPL at MP8, which is 6 m away from the reactor, is approximately 2 dBA lower than that at MP6, which is at the same distance. There is a significant difference in noise levels 1 m inside and outside the fence, with an SPL difference of 14.8 dBA.

Here, we select MP1 for further analysis. **Table 2** presents both the A-weighted and linear-weighted SPLs for mid-to-low frequencies (63–315 Hz) as well as for the full frequency range (20–6300 Hz). Analysis of the data in **Table 2** reveals that the

difference in SPL between considering only mid-low frequencies and the full frequency range is 0.8 dBA and 0.1 dB for A-weighted and linear-weighted levels, respectively. This suggests that the reactor noise is primarily concentrated in the mid-low frequency band of 63–315 Hz. Therefore, the subsequent analysis will exclude high-frequency noise above 315 Hz, focusing on the mid-low frequency band.

Table 2. SPLs at 1 m from the reactor.

Weighting method	**SPL**	
	63–315 Hz	20–6300 Hz
A-weighted	75.7 dBA	76.5 dBA
Linear-weighted	93.5 dB	93.6 dB

Since A-weighting dominantly attenuates the low-frequency noise, and in consideration of the A/C/Z-weighted curves' characteristics [38], the reactor noise is predominantly characterized by 50 Hz harmonics. As a result, linear weighting will be primarily employed for the analysis in this study, while A-weighting can be used to assess whether the noise levels exceed the relevant standards.

2.2. Spectral characteristics

This subsection analyzes spectral characteristics of the reactor noise to identify dominant frequencies and provide a theoretical basis and design objectives for subsequent noise control measures at the switchyard.

2.2.1. 1/3 octave spectrum

Here, the spectral characteristics of the noise in the area near the reactor and the area inside the fence are analyzed to identify the dominant frequencies of the noise within the station. **Figure 3** shows the 1/3 octave spectral characteristics measured at MP1–MP8, which mainly cover the inner side of the fence and the area near the reactor.

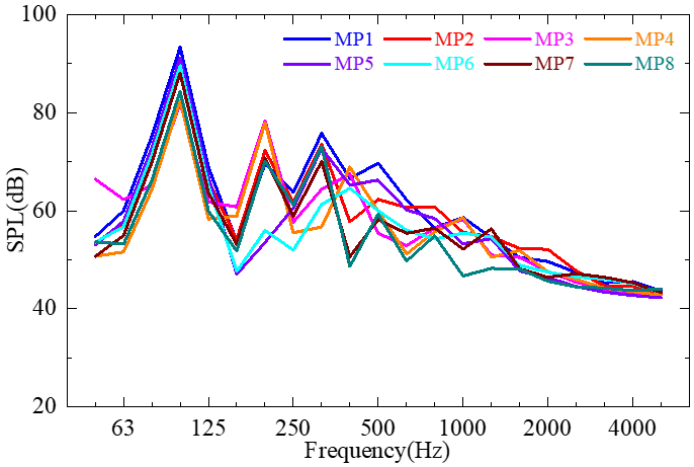

Figure 3. 1/3 octave spectral characteristics of SPLs near the reactor and fence.

Analysis of **Figure 3** reveals that, although there are differences in the amplitude of the SPL near the reactor and the inner side of the fence, the spectral characteristics are essentially the same. The noise is predominantly concentrated in the mid-low

frequency band below 500 Hz, particularly in the frequency bands of 100 Hz, 200 Hz, and 315 Hz, where there are distinct peaks in the SPL. Among these, the frequency band of 100 Hz is the most significant. Additionally, as the frequency increases, the SPL exhibits a trend of gradual attenuation.

To further illustrate the frequency distribution of the noise near the reactor and inside the fence, **Table 3** lists the proportion of noise in each frequency band at MP1–MP8. The data in **Table 3** indicate that the noise at these MPs is primarily concentrated in the 63–315 Hz frequency band, with minimal contributions from frequency bands below 63 Hz and above 315 Hz. Specifically, the noise in the frequency band from 63 Hz to 315 Hz accounts for over 94% of the total noise, while the sum of the noise in the remaining frequency bands is less than 6%. Therefore, in the subsequent research presented in this article, we mainly focus on the noise in the 63–315 Hz band to simplify the noise prediction model and enhance computational efficiency.

Table 3. Proportion of reactor and fence noise in each frequency band.

Frequency Band	MP1	MP2	MP3	MP4	MP5	MP6	MP7	MP8
<63 Hz	0.40%	0.30%	3.50%	0.80%	0.30%	0.60%	0.10%	0.40%
63–315 Hz	98.9%	99.3%	94.1%	95.2%	99.0%	98.9%	99.6%	98.9%
>315 Hz	0.8%	0.5%	3.0%	4.0%	0.7%	0.6%	0.4%	0.8%

2.2.2. Narrowband spectrum

The narrowband spectral characteristics of the noise near the reactor and inside the fence are analyzed here. **Figure 4** presents the narrowband spectral characteristics measured at MP1–MP8. As indicated in the previous section, the noise near the reactor and inside the fence is primarily concentrated in the mid-low frequency bands. Therefore, only the narrowband spectrum curves of the SPL up to 1000 Hz are presented here.

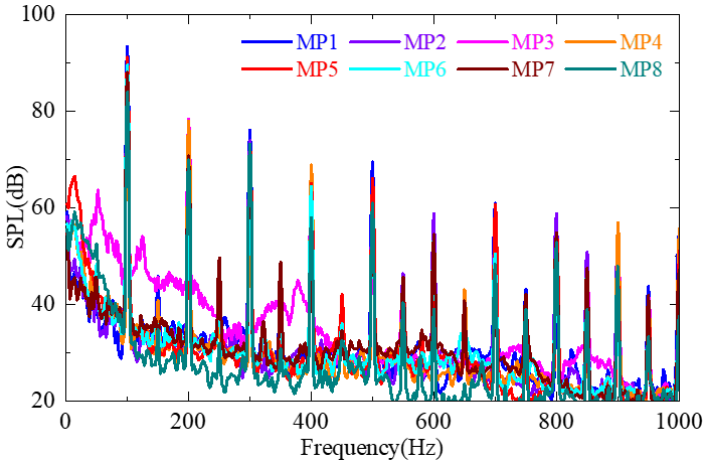

Figure 4. Narrowband spectral characteristics of SPLs near the reactor and fence.

Analysis of **Figure 4** reveals that the noise near the reactor and inside the fence exhibits discrete-frequency characteristics and significant tonal characters. At MP1–MP8, the SPL exists with distinct peaks at 100 Hz and its harmonic frequencies, with the most pronounced peak occurring at 100 Hz. Specifically, the SPL at each MP

reaches its maximum value at 100 Hz. Additionally, as the frequency increases, the SPL peak at the harmonic frequencies exhibits a gradual attenuation trend.

The SPL peaks at 100 Hz, and its harmonic frequencies for each MP are presented in **Table 4**. As shown in the table, specific values of the SPL at each MP vary between 82 dB and 93.3 dB at 100 Hz, which is identified as the dominant frequency of the noise near the reactor and inside the fence. Additionally, the SPL peak at MP5 is higher than that of MP3, MP4, MP6, and MP7 at most peak frequencies. Particularly for MP3 and MP4, which are closer to the reactor, the SPL at MP5 is notably higher at 100 Hz, 300 Hz, 500 Hz, 600 Hz, 700 Hz, and 800 Hz. At the significant frequency of 100 Hz, the SPL at MP5 is approximately 8.6–9.1 dB higher than that at MP3 and MP4. Since the half-wavelength of the sound wave at 100 Hz is calculated to be 1.7 m. The distance of the 4th wave node is 1.7 m × 3 = 5.1 m, and MP5 is located near this 4th wave node. At the wave node, air molecules are compressed, resulting in an increase in sound pressure.

Table 4. SPLs at 100 Hz and harmonic frequencies at each MP (dB).

Frequency (Hz)	MP1	MP2	MP3	MP4	MP5	MP6	MP7	MP8
100	93.3	90.6	82.0	82.5	91.1	89.5	88.0	83.9
200	69.5	72.2	78.4	77.9	52.9	55.6	70.7	69.9
300	76.1	73.9	64.5	55.9	73.0	61.2	70.4	73.1
400	66.3	57.1	67.2	68.8	65.0	64.4	47.2	57.9
500	69.5	61.9	53.7	59.3	66.0	59.5	57.5	60.9
600	58.2	58.8	45.0	47.6	50.0	54.2	54.4	38.9
700	60.9	56.3	52.3	45.7	60.6	50.4	42.4	48.3
800	42.0	58.8	51.8	52.3	54.8	51.1	54.8	52.8
900	51.6	52.8	56.4	56.9	44.9	42.2	47.3	47.9
1000	54.9	47.6	54.8	55.7	51.1	42.9	47.2	37.4

3. Noise prediction model

Based on the measured noise data from the reactor presented in Section 2, the sound pressure amplitude at 1 m from the reactor is used as the input acoustic source for the model. To account for multiple acoustic sources, three reactor sets and the firewall are included in the prediction model as additional acoustic sources.

3.1. Calculation parameters

The prediction model includes the characteristics of the acoustic sources, absorption conditions, and the geometric parameters of both the reactor and noise barriers, including the top structures. The air density is set to 1.21 kg/m^3, and the speed of sound in air is 344 m/s. For linear boundary element models, to ensure calculation accuracy, the length of each element must be less than one-sixth of the shortest wavelength corresponding to the calculated frequency [39]. Given that the frequency range considered in this study is 20–360 Hz, the element length is set to 0.158 m, which satisfies the following condition.

$$0.158\text{m} < \frac{344}{6 \times 360}\text{m} \tag{1}$$

3.1.1. Acoustic source

The equivalent method for the acoustic source of a transformer in reference [22] treats the acoustic source as a plane source. It ultimately converts the source into multiple point sources by replacing the plane source with several point sources and represents the source strength of each equivalent source using the sound power level. This equivalent method requires measuring the SPL at only a few field points near the transformer. Therefore, based on the noise data measured near the reactor in Section 2, the actual noise data within 2 m of the reactor are primarily used. In this area, the influence of the noise from adjacent reactors can be neglected due to the shielding effect of the firewall, allowing for a simplified representation of the reactor acoustic source.

In this study, we ignore the vibration radiation noise from the top and bottom of the reactor and assume that the reactor noise mainly originates from the vibration of the other four side walls. Thus, the reactor can be equivalently represented as four plane sources. After replacing the plane source with point sources, the reactor is ultimately modeled as multiple point sources.

It is assumed that the surface sound pressure of the plane source on the four sides of the reactor is uniform. The sound field calculation formula for the plane source is given in reference [40].

$$L_{\text{p}} = L_{\text{pm}} - 8 + 10\text{lg}\left(\int_{l_1}^{l_2}\int_{w_1}^{w_2} \frac{\text{d}x\text{d}y}{(x-a)^2 + (y-b)^2 + (z-d)^2}\right) \tag{2}$$

where (a, b, d) are the coordinates of the field point. l_1, l_2, w_1, and w_2 are the starting and ending coordinates of the length and width of the plane source, respectively. L_{p} is the SPL of the field point, and L_{pm} is the average SPL of the plane source.

In order to facilitate the calculation of outdoor substation noise and simplify the equivalent process, the source intensity of the point source is expressed as sound power level. The calculation formula for the SPL of each point in the radiated sound field can be expressed as

$$L_{\text{p}} = I_{\text{w}} - 20\text{lg}r - 1 \tag{3}$$

where I_{w} is the sound power level of the point source, and r is the distance between the source and the field point.

To simplify the computational complexity and ensure the accuracy of the sound field for equivalent sources, it is assumed here that there are 9 equivalent sources [22]. Following the energy superposition method, the total SPL generated by these equivalent sources at the field point x is

$$L = 10\text{lg}\left(\sum_{i=1}^{9} 10^{0.1(L_{\text{w}}(i) - 20\text{lg}R(i) - 11)}\right) \tag{4}$$

where L_{w} represents a 1 × 9 matrix consisting of the sound power levels of 9 point sources, and $R(i)$ denotes the distance between the ith point source and the field point x. And $R = [R(1), R(2), \cdots, R(9)]$ is defined as a 1×9 matrix consisting of the distances between 9 point sources and the field point x.

When the SPLs of M field points are known, the equation can be obtained.

$$L(j) = 10\lg\left(\sum_{i=1}^{9} 10^{0.1\left(L_{\mathrm{w}}(i) - 20\lg R_j(i) - 11\right)}\right), j = 1,2,\cdots,M \tag{5}$$

If M ≥ 9, the genetic algorithm can be used to solve L_{w}, which is the sound power level of 9 equivalent sources.

3.1.2. Geometric parameter

The study examines the effects of fence height, top structures, noise barriers (including top structures), and sound-absorbing materials on the acoustic field around the reactor and fence. The prediction model for the reactor noise is presented in **Figure 5**. In the model, the ground, fence, firewall, reactor, and noise barriers are assumed to be acoustically rigid surfaces, with wave reflections between the reactor, ground, fence, and firewall considered. The reactor unit measures 5.7 m in length, 5.9 m in width, and 4 m in height, while the existing fence is 5 m high and situated 3.5 m from the firewall.

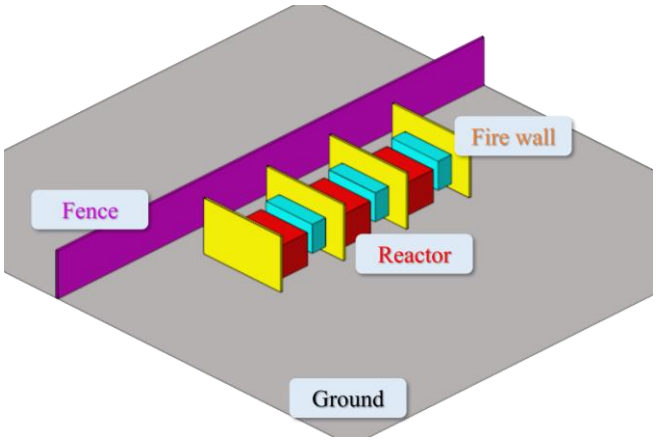

Figure 5. Acoustic BEM prediction model.

A group of three-phase reactors is considered in this model. While simplifying the model to facilitate calculation, the acoustic interference effect of the noise from the adjacent phase reactors on the acoustic evaluation points in the area near the middle reactor is taken into account.

3.1.3. Absorption condition

The absorption coefficients of sound-absorbing materials or structures can be measured using impedance tubes or reverberation chambers. However, in BEM calculations, absorption characteristics are defined by acoustic impedance. Consequently, the absorption coefficients must be converted into acoustic impedance.

The absorption coefficient α can be defined as [41]

$$\alpha(f) = 1 - \left|\frac{Z\cos(\theta) - \rho_0 c_0}{Z\cos(\theta) + \rho_0 c_0}\right| \tag{6}$$

where θ represents the angle of the incidence wave, Z represents the acoustic impedance ratio, and $\rho_0 c_0$ represents the characteristic impedance of air. Here, the normal absorption coefficient is used instead of the reverberation absorption coefficient; that is, $\theta = 0$.

Using the Attenborough's dual-parameter impedance model [42], we can get

$$Z = 0.436(1+i)\sqrt{\frac{\sigma_e}{f}} + 19.74i\frac{\alpha_e}{f} \tag{7}$$

in which σ_e represents the characteristic flow resistance of the material, α_e represents the various porosity of the porous material, and f represents the frequency. By changing the values of σ_e and α_e in the numerical model, the real and imaginary parts of the acoustic surface impedance of the material can be changed to make it equivalent to the measured absorption coefficient.

Figure 6 shows the absorption coefficients of three traditional sound-absorbing materials at center frequencies of the 1/3 octave band, including Glass Wool (30 mm), Melamine (36 mm), and Carbon Fiber (50 mm). It can be found that the absorption performance of traditional materials is mainly concentrated in the high-frequency band (≥1000 Hz). For the mid-low frequency noise within 1000 Hz, especially the low-frequency noise within 315 Hz, the absorption effect is poor.

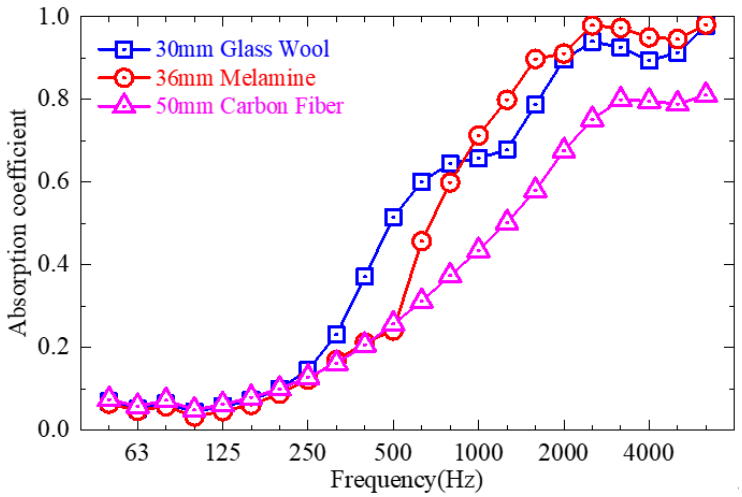

Figure 6. 1/3 octave spectral characteristics of absorption coefficients.

In this study, acoustic boundary conditions are primarily applied to the inner side of the fence, the surface of the firewall, and the body of the noise barriers to investigate the impact of absorption on NREs.

3.2. Evaluation points

To comprehensively evaluate the NRE of measures such as increasing the height of the fence, installing additional barriers (including top structures), and applying sound-absorbing materials in the acoustic field near the fence and reactor, evaluation

points at varying distances and heights are selected. The IL values are then calculated and averaged.

The evaluation points are divided into five zones along the cross-section of the fence and reactor: the far-field and near-field zones outside the fence, the zone between the fence and reactor, and the near-field and far-field zones on the side of the reactor opposite the fence.

- In the far-field and near-field zones outside the fence, three positions are selected at distances of 1 m, 3 m, and 8 m from the fence.
- In the zone between the fence and reactor, two positions are selected at distances of 1 m and 3 m from the fence.
- On the side of the reactor opposite the fence, three positions are selected at distances of 1 m, 5 m, and 10 m from the reactor.

Four heights are selected in each zone: 1.5 m, 3 m, 5 m, and 8 m. **Figure 7** illustrates the layout of the evaluation points. This arrangement enables a comprehensive assessment of the NREs of the measures on the acoustic field near the fence and reactor.

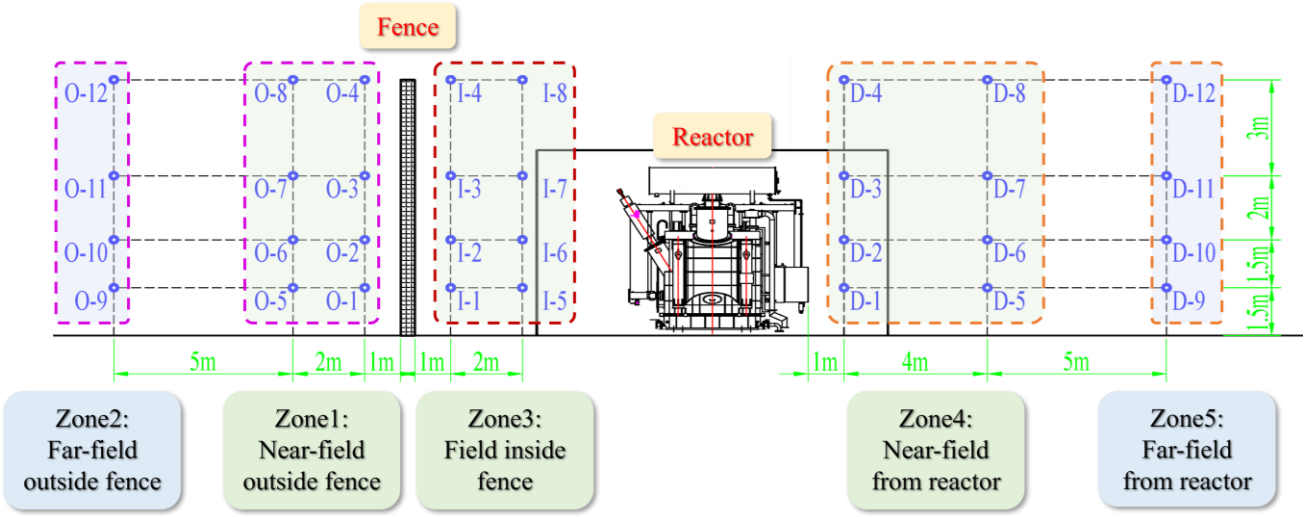

Figure 7. Layout diagram of acoustic evaluation points.

3.3. Calculation scenarios

Using the established noise prediction model, the noise levels near the reactor and fence are calculated for various scenarios, including the increase in fence height, the installation of additional noise barriers, the addition of top structures, and the application of sound-absorbing materials.

Firstly, the impact of increasing the fence height on the noise levels near the reactor and fence is investigated. The current fence height is 5 m, and the effects of raising the height to 5.5, 6, 6.5, and 7 m are examined. Subsequently, the effects of installing an additional noise barrier between the reactor and fence are analyzed, considering both the barrier height and its distance from the firewall. The specific calculation scenarios are presented in **Table 5**.

Table 5. Calculation scenarios for NRE of erect noise barriers.

Case No.	Distance (D/m)	Height (H/m)	Case No.	Distance (D/m)	Height (H/m)
1	1		4		3
2	2	5	5	1	4
3	3		6		6
			7		7

Furthermore, the model is used to compare the additional NREs of several common top structures, as shown in **Figure 8**. The overall height of the noise barriers is maintained at 5 m.

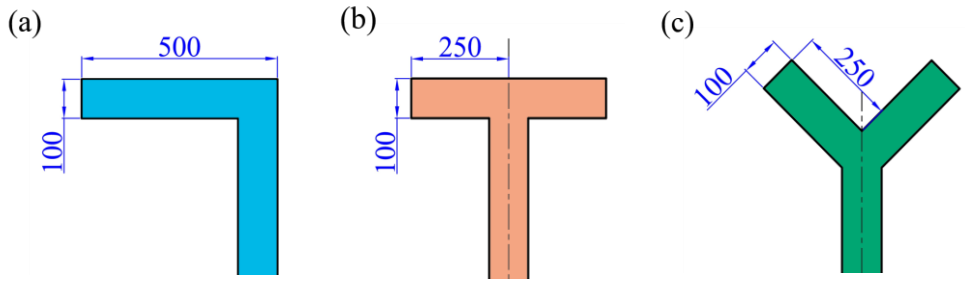

(a) **(b)** **(c)**

Figure 8. Cross-section of top structures (mm). **(a)** L-type; **(b)** T-type; **(c)** Y-type.

3.4. Model validation

Using the prediction model described in Section 2.1, the noise distribution near the reactor and fence is calculated and compared with measured data to verify the model's effectiveness and accuracy. This subsection verifies the noise prediction model mainly from two aspects: noise levels and spectral characteristics (including 1/3 octave and narrowband). **Table 6** presents a comparison of the measured (Mea.) and predicted (Pre.) noise levels near the reactor and fence.

Table 6. Comparison of measured and predicted noise levels near the reactor and fence (dB).

MP	MP1	MP2	MP3	MP4	MP5	MP6	MP7	MP8
Mea. SPL	93.6	90.9	84.0	84.1	91.4	89.7	88.3	84.3
Pre. SPL	92.1	92.9	87.3	87.1	91.9	90.3	89.0	84.3

The results indicate that at MP1–MP8, the predicted results of the SPL are within 4 dB of the measured data, with the relative error of the linear-weighted SPL being less than 5%. This indicates that the model demonstrates certain effectiveness and accuracy in predicting the noise levels near the reactor and inside the fence.

Additionally, we compare the predicted and measured SPL spectral characteristics in this section, with MP1 and MP8 selected as representatives for analysis. **Figure 9a** presents the 1/3 octave spectral characteristic curves of the SPL at MP1 and MP8 within the primary noise frequency band (≤315 Hz). In this figure, symbols with a solid line represent the measured data, while symbols with a dotted line represent the predicted results. Although there are differences between the predicted and measured SPL amplitudes in each frequency band at MP1 and MP8, the

predicted results are generally consistent with the measured data in terms of spectral characteristics, such as the primary frequency band of noise and the trend of SPL changes in each frequency band. Particularly in the frequency band of 100 Hz, the measured and predicted SPLs at MP1 and MP8 are within 2 dB. This demonstrates that the noise prediction model has a certain level of effectiveness and accuracy in reproducing the spectral characteristics of noise near the reactor and inside the fence.

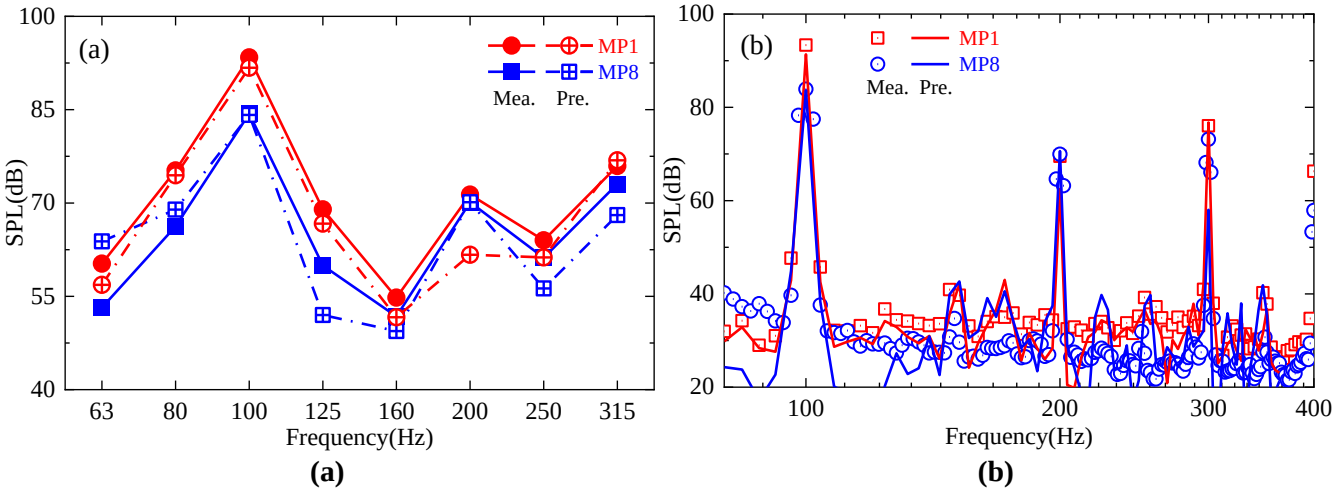

(a) **(b)**

Figure 9. Spectral characteristics of measured and predicted SPLs. **(a)** 1/3 octave; **(b)** Narrowband.

Similarly, the narrowband spectral characteristics of the SPL at MP1 and MP8 are presented in **Figure 9b**. In this figure, symbols denote the measured data, and solid lines represent the predicted results. It is evident that the narrowband spectral characteristics of the SPL obtained from measurements and simulations at MP1 and MP8 are essentially consistent, with obvious SPL peaks appearing at 100 Hz, 200 Hz, and 300 Hz. Particularly at 100 Hz, the measured and predicted SPLs at MP1 and MP8 are within 2 dB. This further demonstrates that the noise prediction model established in this study is effective and accurate in reflecting the noise spectral characteristics, especially in the narrowband range.

4. Analysis of predicted results

4.1. NRE of fence measures

Without the addition of noise barriers or sound-absorbing materials, the noise level outside the fence can be reduced by increasing the height of the fence or by adding structures on its top. This subsection first investigates the impact of different fence heights and top structures on noise outside the fence.

4.1.1. Different fence heights

First, the impact of increasing the fence height on the noise levels near the reactor and fence was investigated. In the switchyard investigated in this study, the existing fence near the reactor is approximately 5 m high. Here, we explore the effects of increasing its height to 5.5 m, 6 m, 6.5 m, and 7 m. The noise prediction model established in the previous section is employed to calculate the noise levels in the areas near the reactor and fence. **Table 7** presents the NREs of increasing the fence height

in different zones near the reactor and fence. Positive values indicate a reduction in the average noise level in the area, while negative values indicate an increase.

Table 7. NREs of increasing the fence height (dB).

Fence Height	Zone 1	Zone 2	Zone 3	Zone 4	Zone 5
5.5 m	−2.5	−1.1	0.1	0.0	0.0
6.0 m	3.8	5.5	0.9	0.1	0.4
6.5 m	5.8	3.3	0.5	−0.1	0.1
7.0 m	3.9	1.0	0.4	−0.2	−0.2

Analysis of the data in **Table 7** reveals that increasing the fence height can effectively reduce the noise level in the areas outside the fence (Zone 1 and Zone 2), while having minimal impact on the noise levels in the areas inside the fence (Zone 3) and near the reactor (Zone 4 and Zone 5), with NREs generally less than 1 dB. As the fence height increases, sound wave diffraction over the fence becomes more difficult, leading to improved NREs outside the fence. However, when the fence height is increased to 5.5 m, the noise level in the area outside the fence increases by 1.1–2.5 dB. When the fence height reaches 7 m, the NREs do not further improve compared to those with a height of 6.5 m.

To further elucidate this phenomenon, additional analysis is conducted here, incorporating the noise spectral characteristics at the evaluation points (EP). EPs O-1 and O-9, located in the near-field and far-field areas outside the fence, are selected as examples for analysis. **Figure 10a** shows the 1/3 octave spectral characteristic curves of the SPL at EPs O-1 and O-9 when the fence height is 5 m and 5.5 m, respectively. As shown in this figure, when the fence height increases from 5 m to 5.5 m, the SPLs at EPs O-1 and O-9 decrease in most frequency bands. However, in the frequency band of 100 Hz, the SPLs at these two EPs increase by 10 dB and 7 dB, respectively. This is the main factor contributing to the increased noise level in the area outside the fence.

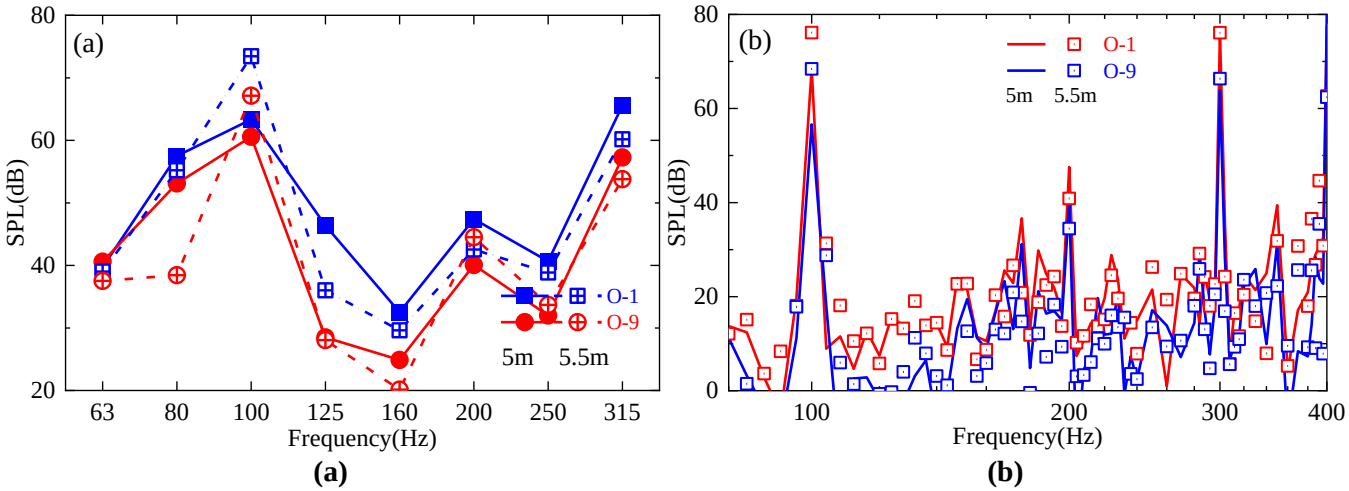

(a) **(b)**

Figure 10. Spectral characteristics of SPLs before and after increasing fence height. **(a)** 1/3 octave; **(b)** Narrowband.

In addition, the narrowband spectral characteristics of the SPL at EPs O-1 and O-9 are presented here for auxiliary explanation, as shown in **Figure 10b**. It can be seen

that at the noise significant frequency of 100 Hz, the increase of the fence height from 5 m to 5.5 m will increase the SPL at the two EPs by 7–11 dB.

To provide further insight, the vertical distribution of the SPL at 100 Hz for different fence heights is shown in **Figure 11**. The shaded areas in the figure represent solid structures such as the reactor, firewall, and fence. The color gradient indicates the noise levels, with darker blue denoting lower noise levels and darker red denoting higher noise levels.

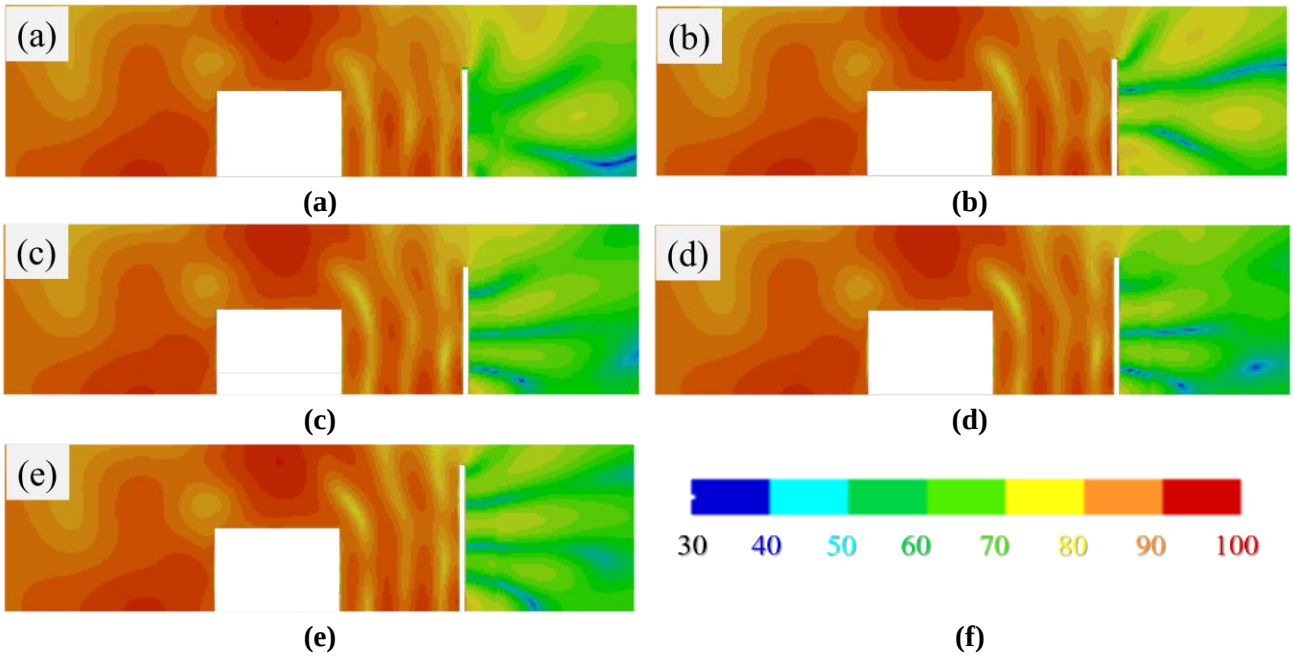

(a) **(b)** **(c)** **(d)** **(e)** **(f)**

Figure 11. Cloud diagram of SPL distribution for different fence heights (100 Hz). **(a)** 5 m; **(b)** 5.5 m; **(c)** 6 m; **(d)** 6.5 m; **(e)** 7 m.

As shown in this figure, the noise level outside the fence at 100 Hz generally decreases as the fence height increases. In contrast, the noise levels inside the fence and near the reactor remain relatively unchanged. However, when the fence height is 5.5 m, the area outside the fence exhibits pronounced acoustic modal characteristics, leading to a significant increase in noise levels in this region. Additionally, when the fence height reaches 7 m, the noise level outside the fence does not decrease significantly compared to when the height is 6.5 m.

4.1.2. Adding top structures

The impact of top structures for the fence (while keeping the fence height constant) on NREs was investigated. Three common top structures—L-type, T-type, and Y-type—were considered, as shown in **Figure 8**. **Table 8** shows the additional NREs of these structures in different zones.

Table 8. Additional NREs of adding top structures for the fence (dB).

Top Structure	Zone 1	Zone 2	Zone 3	Zone 4	Zone 5
L−type	2.8	−0.8	0.0	0.0	0.0
T−type	0.4	4.6	0.2	0.0	0.0
Y−type	−0.2	−0.1	0.0	0.0	−0.1

The results indicate that adding top structures to the fence has a minimal impact on noise levels inside the fence and near the reactor but has varying effects on noise levels outside the fence.

Specifically, the L-type top structure leads to a significant noise reduction in Zone 1 outside the fence, reducing the SPL by an average of 2.8 dB, while the SPL in Zone 2 increases by 0.8 dB. The T-type top structure demonstrates the best NRE in Zone 2 outside the fence, decreasing the SPL by an average of 4.6 dB, with minimal change in Zone 1. The Y-type top structure has little effect on the noise levels outside the fence.

4.2. An additional noise barrier

This subsection examines the NRE of installing an additional noise barrier between the reactor and fence. The precise location of the barrier is depicted in **Figure 12**. The primary parameters of the barrier are the horizontal distance, *D*, from the firewall and its vertical height, *H*, with the longitudinal length matching that of the fence.

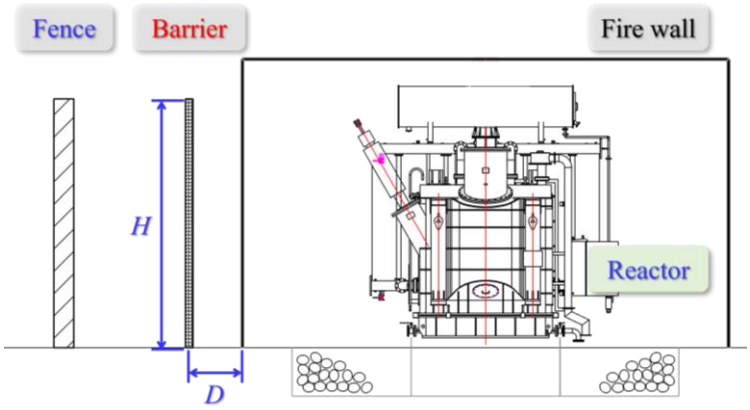

Figure 12. Layout diagram of the additional noise barrier.

4.2.1. Different distance from firewall

The effect of the distance between the additional erected noise barrier and the firewall on the acoustic field near the reactor and fence was examined. A noise barrier with a height of 5 m was installed at distances of 1 m, 2 m, and 3 m from the firewall. **Table 9** presents the average ILs of the noise barrier at these distances.

Table 9. Average ILs of the erect barrier at different distances (dB).

Distance	Zone 1	Zone 2	Zone 4	Zone 5
1 m	8.1	8.1	0.8	2.6
2 m	1.4	8.8	0.2	1.7
3 m	2.1	2.7	1.2	2.0

The analysis of the data indicates that installing a noise barrier between the reactor and fence can effectively reduce noise levels in various zones. The optimal NRE is achieved when the barrier is positioned 1 m from the firewall. Under these

conditions, the SPL in Zone 1 and Zone 2 outside the fence decreases by an average of 8.1 dB, while the SPL near the reactor is reduced by 0.8 to 2.6 dB.

To further illustrate this, the vertical distribution of the SPL before and after the installation of the noise barrier is shown in **Figure 13**. The results demonstrate that installing a noise barrier 1 m from the firewall dominantly reduces the noise level outside the fence while providing only minimal noise reduction near the reactor.

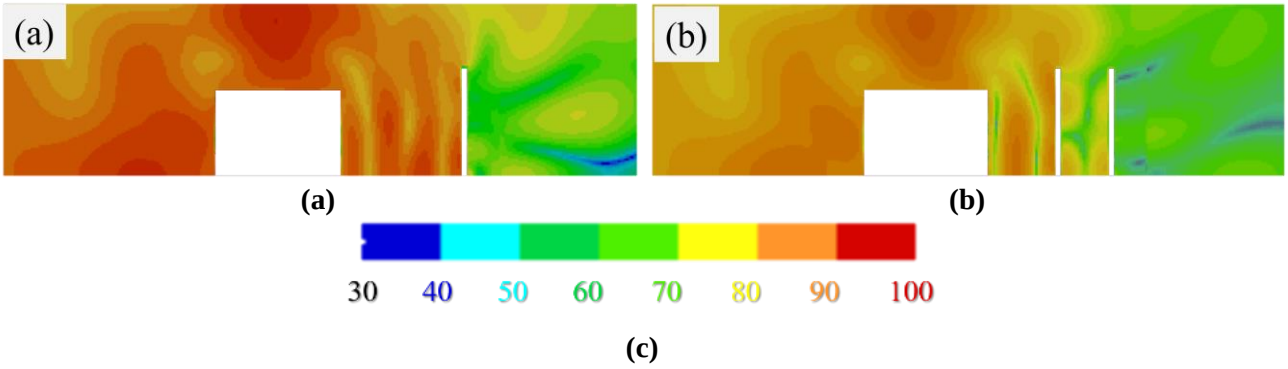

Figure 13. Cloud diagram of SPL distribution in the vertical direction before and after installing the barrier. **(a)** without a barrier; **(b)** with an erect barrier.

4.2.2. Different barrier heights

The impact of the height of an additional erect noise barrier on the noise levels outside the fence and near the reactor is investigated here. The distance between the erect noise barrier and the firewall is maintained at 1 m. **Table 10** presents the average IL of vertical noise barriers with different heights in the areas outside the fence and near the reactor. Data analysis reveals that increasing the height of the barrier significantly enhances the average IL outside the fence while having minimal impact on the average IL near the reactor. For each 1-m increase in the height of the barrier, the average IL in the area outside the fence (Zone 1 and Zone 2) increases by 0.7–2.2 dB and 0.6–3 dB, respectively, while the average IL in the area near the reactor (Zone 4 and Zone 5) changes within 0.3 dB. When the height of the additional erect noise barrier is increased to 7 m, the average IL in the area outside the fence is maximized, reaching 11.0–11.9 dB.

Table 10. Average ILs of the erect barrier with different heights (dB).

Height	Zone 1	Zone 2	Zone 4	Zone 5
3 m	4.8	4.5	0.6	2.7
4 m	6.2	7.5	0.6	2.8
5 m	8.1	8.1	0.8	2.6
6 m	8.8	10.8	0.8	2.9
7 m	11.0	11.9	0.8	2.6

Here we provide further explanation in conjunction with the vertical distribution of the SPL. **Figure 14** shows the SPL distribution cloud diagram after adding 5-m-high and 7-m-high erect barriers. The results indicate that increasing the height of the

noise barrier from 5 m to 7 m effectively reduces the noise level in the shadow area behind the barrier but has little effect on the noise level near the reactor.

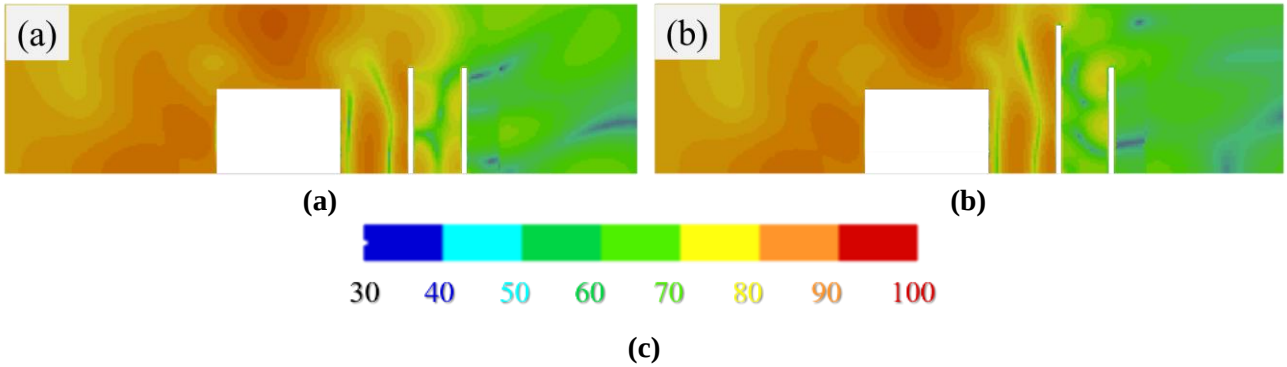

Figure 14. Cloud diagram of SPL distribution in the vertical direction for erect barriers with different heights. **(a)** 5 m; **(b)** 7 m.

4.2.3. Adding top structures

The effect of adding top structures to the additional erected noise barrier on the NRE was investigated. A 5 m high noise barrier, erected 1 m from the firewall, was supplemented with three top structures: L-type, T-type, and Y-type. The overall height of the barrier remained 5 m. **Table 11** presents the additional NREs of these top structures in comparison to a barrier of the same height without the top structures.

Table 11. Additional NREs of top structures for the barrier (dB).

Top Structure	Zone 1	Zone 2	Zone 4	Zone 5
L-type	−0.1	0.6	0.0	0.0
T-type	1.6	1.8	0.0	0.1
Y-type	1.0	1.0	0.0	0.1

The results indicate that adding top structures to the erected noise barrier enhances the NRE, particularly outside the fence. Among these top structures, the T-type provides the most dominant additional NRE, reducing the SPL by 1.6–1.8 dB in Zones 1 and 2 outside the fence. The Y-type top structure offers slightly less NRE, with a reduction in SPL of 1.0 dB, while the L-type top structure has a minimal effect.

4.3. Sound-absorbing materials

This section investigates the impact of traditional sound-absorbing materials in Section 3.1 on the acoustic field near the reactor and fence. These materials are primarily applied to the inner side of the fence, the surface of the firewall, and the inner side of the additional erected noise barrier.

4.3.1. Applying to the fence

First, the impact of applying sound-absorbing materials to the inner side of the fence on noise levels near the reactor and fence was investigated. **Table 12** presents the additional NREs for these materials compared to an acoustic rigid fence.

Table 12. Additional NREs after applying sound-absorbing materials to the fence (dB).

Material	Zone 1	Zone 2	Zone 3	Zone 4	Zone 5
Glass Wool	0.1	1.1	0.2	0.1	0.2
Melamine	0.1	0.8	0.1	0.1	0.1
Carbon Fiber	0.1	1.2	0.2	0.1	0.2

Data analysis indicates that applying sound-absorbing materials to the inner side of the fence has minimal impact on noise levels inside the fence and near the reactor, with NREs varying within 0.2 dB. For the far-field area outside the fence (Zone 2), sound-absorbing materials can achieve an additional noise reduction of 0.8–1.2 dB. However, for the near-field area outside the fence (Zone 1), sound-absorbing materials also have minimal effect on the noise level. Additionally, Glass Wool and Carbon Fiber exhibit slightly better noise reduction performance compared to Melamine.

Here, we further analyze the noise spectral characteristics at the EPs, selecting EPs O-1 and O-9 in the near-field and far-field areas outside the fence, as well as EP I-1 in the inner area of the fence, as examples for analysis. **Figure 15a** shows the 1/3 octave spectral characteristic curves of the SPL at EPs before and after installing Glass Wool inside the fence. As shown in **Figure 15a**, after the installation of Glass Wool inside the fence, the SPL in the primary noise frequency band (≤315 Hz) at EPs O-1, O-9, and I-1 cannot be effectively reduced, particularly in the significant noise frequency band of 100 Hz. Combined with the absorption coefficient spectral characteristics shown in **Figure 6**, it is evident that traditional sound-absorbing materials have poor absorption effects on mid-low frequency noise, especially below 315 Hz. This explains why the installation of traditional sound-absorbing materials inside the fence has minimal impact on NREs inside the fence and near the reactor.

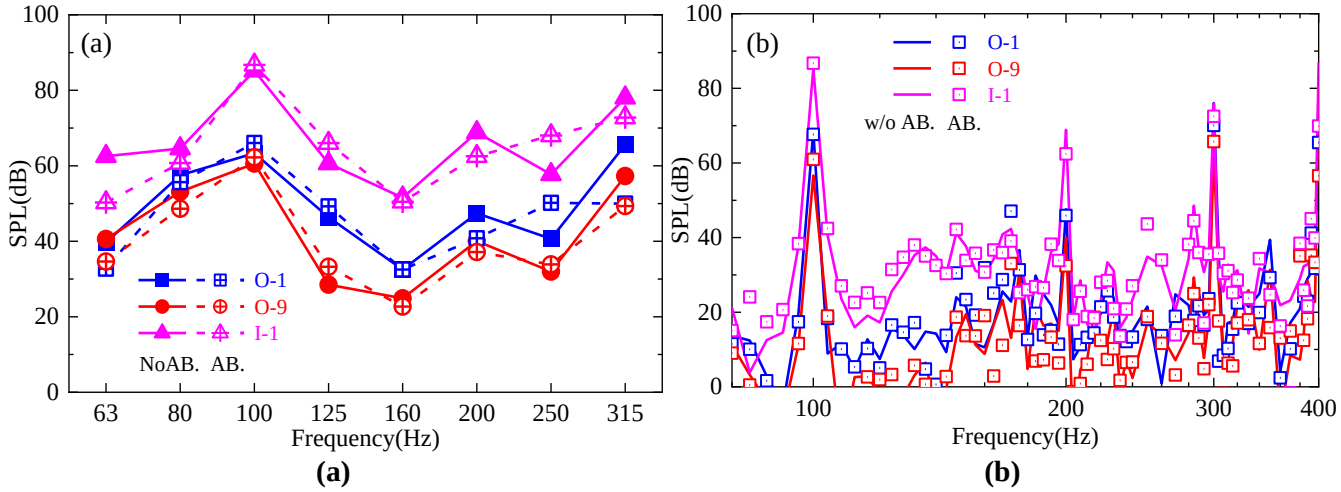

Figure 15. Spectral characteristics of SPLs before and after applying Glass Wool to the fence. **(a)** 1/3 octave; **(b)** narrowband.

In addition, the narrowband spectral characteristics of the SPL at EPs O-1, O-9, and I-1 are given here for auxiliary explanation, as shown in **Figure 15b**. It can be

seen that installing Glass Wool on the inner side of the fence cannot effectively reduce the SPL at these EPs at the noise-significant frequency of 100 Hz.

4.3.2. Applying to the firewall

The effect of applying sound-absorbing materials to the surface of the firewall on noise levels near the reactor and fence was also investigated. The materials considered are identical to those used for the fence. **Table 13** presents the additional NREs of these materials in comparison to those of an acoustically rigid firewall.

Table 13. Additional NREs after applying sound-absorbing materials to the firewall (dB).

Material	Zone 1	Zone 2	Zone 3	Zone 4	Zone 5
Glass Wool	−0.1	0.9	0.2	0.3	0.6
Melamine	−0.1	0.6	0.1	0.2	0.4
Carbon Fiber	−0.1	1.0	0.2	0.3	0.6

The results indicate that applying sound-absorbing materials to the firewall has a minimal effect on the noise levels near both the reactor and fence. When compared to the application of materials to the fence, using sound-absorbing materials on the firewall results in a slightly greater noise reduction near the reactor, by 0.2–0.4 dB.

4.3.3. Applying to the noise barriers

The effect of applying sound-absorbing materials to the inner side of the additional erected noise barrier on noise levels was investigated. The sound-absorbing materials considered are the same as those used for the fence. **Table 14** presents the additional NREs of these materials in comparison to an acoustically rigid erect barrier. Analysis of the data reveals that applying sound-absorbing materials to the inner side of erect noise barriers results in additional NREs of 0.7–1.7 dB near the reactor. However, these materials lead to a reduction in NREs in Zone 1 outside the fence by 0.5–2.1 dB. Melamine and Carbon Fiber improve the NREs in Zone 2 outside the fence by 1.7 dB.

Table 14. Additional NREs after applying sound-absorbing materials to the barrier (dB).

Material	Zone 1	Zone 2	Zone 4	Zone 5
Glass Wool	−0.5	−0.1	0.7	1.7
Melamine	−2.1	1.7	0.7	1.6
Carbon Fiber	−2.1	1.7	0.7	1.6

The impact of traditional sound-absorbing materials on the NRE is minimal in this application. The reasons are as follows: First, the HV switchyard investigated in this study is an open environment, with the reactor arranged outdoors. In such an environment, the reactor noise propagates freely in all directions. The space where sound-absorbing materials work is limited, and the actual effect is not as good as in a closed space. Second, field testing data indicate that the reactor noise is primarily concentrated in the mid-low frequency bands below 315 Hz. The absorption

coefficient of traditional sound-absorbing materials in this frequency band is typically less than 0.3 (see **Figure 6**), resulting in poor absorption of the reactor noise. This situation could be improved by employing acoustic metamaterials, which exhibit excellent sound absorption effects in the mid-low frequency bands.

5. Conclusions

This study developed a noise prediction model for the HV reactor in a ±500 kV HV switchyard and examined the effects of fence height, additional noise barriers, top structures, and sound-absorbing materials on the noise reduction effect. The main conclusions are as follows:

a) Increasing the height of the fence by 1–2 m can reduce noise levels outside the fence by 1–5.8 dB, and the best effect is achieved when the height is 6/6.5 m. Adding L-type and T-type top structures to the fence can further reduce the noise levels by 2.8 dB and 0.4–4.6 dB, respectively.

b) Installing an additional noise barrier between the reactor and fence, 1 m away from the firewall, can reduce noise levels outside the fence and near the reactor by 4.5–11.9 dB and 0.6–2.9 dB, respectively. The best effect is achieved when the height is 7 m.

c) Adding T-type and Y-type top structures to a 5-m-high noise barrier, positioned 1 m from the firewall, can further reduce noise levels outside the fence by 1–1.8 dB, with minimal impact on noise levels near the reactor.

d) Applying traditional sound-absorbing materials to the fence or firewall has a minimal effect on noise levels near both the fence and the reactor, with additional NRE of less than 1.2 dB. Applying these materials to the additional noise barrier can further reduce noise levels near the reactor by 0.7–1.7 dB.

Author contributions: Conceptualization, LL, SX, XD and XX; methodology, SX, MW and CZ; software, SX and CZ; validation, SX, CZ and WM; formal analysis, XD, and XX; investigation, SX, CZ and MW; resources, LL, XD and XX; data curation, LL, SX and XX; writing—original draft preparation, LL and SX; writing—review and editing, LL, SX, XD, CZ, MW and XX; visualization, XX; supervision, LL, XD and XX; project administration, LL and XX; funding acquisition, LL and XX. All authors have read and agreed to the published version of the manuscript.

Conflict of interest: The authors declare no conflict of interest.

References

1. Li Z, Lang X, Yang B, et al. Vibration and noise mechanism of a 110 kV transformer under DC bias based on finite element method. Global Energy Interconnection. 2024; 7(4): 503–512. doi: 10.1016/j.gloei.2024.08.012
2. Wang H, Zhang L, Sun Y, Zou L. Research on the influence mechanism of harmonic components on the noise distribution characteristics of converter transformers. International Journal of Electrical Power & Energy Systems. 2024; 160: 110095. doi: 10.1016/j.ijepes.2024.110095
3. Borowik L, Włodarz R, Chwastek K. Eco-efficient control of the cooling systems for power transformers. Journal of Cleaner Production. 2016; 139: 1551–1562. doi: 10.1016/j.jclepro.2015.12.094
4. Di GQ, Zhou XX, Chen XW. Annoyance response to low-frequency noise with tonal components: A case study on transformer noise. Applied Acoustics. 2015; 91: 40–46. doi: 10.1016/j.apacoust.2014.12.003

5. Ying L, Wang D, Wang G, Wang W. Acoustic characteristic analysis of power transformers in urban communities based on a combined finite and boundary element method. Indoor and Built Environment. 2020; 29(2): 208–220.
6. Liang P, Li J, Li Z, et al. Effect of low-frequency noise exposure on cognitive function: a systematic review and meta-analysis. BMC Public Health. 2024; 24(1): 125.
7. Lu Y, Wu SF, Nie C, He W. Locating and reconstructing transformer low-frequency noises with a 3D, six-microphone array. Applied Acoustics. 2025; 228: 110351.
8. Miao X, Jiang P, Pang F, et al. Numerical analysis and experimental research of vibration and noise characteristics of oil-immersed power transformers. Applied Acoustics. 2023; 203: 109189.
9. Piana EA, Roozen NB. On the control of low-frequency audible noise from electrical substations: A case study. Applied Sciences. 2020; 10(2): 637–656.
10. Banks JL, Hubal EAC. Noise: a public health problem. Journal of Exposure Science and Environmental Epidemiology. 2025; 35(1).
11. Hahad O, Kuntic M, Al-Kindi S, et al. Noise and mental health: evidence, mechanisms, and consequences. Journal of Exposure Science & Environmental Epidemiology. 2024; 1–8.
12. Bingham PM. Neurodevelopmental costs of noise pollution-is history rhyming again?. Journal of Exposure Science & Environmental Epidemiology. 2024; 1–3.
13. Mehri A, Abbasi M. Noise exposure and job stress—A structural equation model in textile industries. Archives of Acoustics. 2020; 45(4): 601–611.
14. Zhang J, Wang Y, Chen Y, et al. Estimation method of sound power of UHV transformer based on vibration and sound pressure measurements (Chinese). High Voltage Engineering. 2019; 45(6): 1843–1850. doi: 10.13336/j.1003-6520.hve.20190604021
15. Wang D, Ying L, Jia Y, et al. Noise pollution mitigation method for substations in urban communities based on a smart silencing unit. Journal of Cleaner Production. 2020; 245: 118911. doi: 10.1016/j.jclepro.2019.118911
16. Wang S, Tao J, Qiu X, Burnett IS. A natural ventilation window for transformer noise control based on coiled-up silencers consisting of coupled tubes. Applied Acoustics. 2022; 192: 108744. doi: 10.1016/j.apacoust.2022.108744
17. Rausch M, Kaltenbacher M, Landes H, et al. Combination of finite and boundary element methods in investigation and prediction of load-controlled noise of power transformers. Journal of Sound and Vibration. 2002; 250(2): 323–338. doi: 10.1006/jsvi.2001.3934
18. Wang L, Geng M, Bai X, et al. Urban 110 kV indoor substation noise analysis and control schemes: A real case study. Applied Acoustics. 2021; 183: 108290. doi: 10.1016/j.apacoust.2021.108290
19. Fan X, Li L, Zhao L, et al. Environmental noise pollution control of substation by passive vibration and acoustic reduction strategies. Applied Acoustics. 2020; 165: 107305. doi: 10.1016/j.apacoust.2020.107305
20. Di G, Jiang H, Chen C, et al. A study on the control indices and emission limits of substation noise. Applied Acoustics. 2023; 205: 109275. doi: 10.1016/j.apacoust.2023.109275
21. Oliveira TDA, Acosta JJG, Cunha B, et al. Assessment of the acoustic field in the vicinity of urban high-voltage substations. Measurement: Sensors. 2021; 18: 100162.
22. Sun T, Pei C, Hu J, et al. Noise source model and simulation analysis of UHV transformer. High Voltage Engineering. 2014; 40(9): 2750–2756.
23. Ruan X, Wei H, Li Z. Model for predicting outdoor coherent noise and its engineering application. China Environmental Science. 2015; 35(6): 1877–1884.
24. Gao Y. Research on the acoustic field characteristics and noise distribution prediction of substations [Master's thesis] (Chinese). Beijing: North China Electric Power University; 2014.
25. Wang X, Li W, Jin D. Research progress of noise control technology of substation. Electric Power Technology and Environmental Protection. 2017; 33(6): 34–37.
26. Shi X, Lin Q, Kim J, et al. Optimization of noise control schemes based on improvement of annoyance (Chinese). China Environmental Science. 2018; 39(1): 397–401. doi: 10.19674/j.cnki.issn1000-6923.2019.0049
27. Zhao X, Shuai Z, Zhang Y, Liu Z. Research on design method of metamaterial sound field control barrier based on transformer vibration and noise (Chinese). Energy Reports. 2022; 8: 1080–1089. doi: 10.19674/j.cnki.issn1000-6923.2019.0049

28. Cao M, Mo J, Mo H, et al. Correlation analysis and prediction method on structure vibration and noise caused by transformer in underground substation. In: Proceedings of the CSEE; 2014.
29. Yu S, Fu J, Cha Y. Noise analysis and low-noise design of power transformer (Chinese). Transformer. 2019; 56(9): 19–27. doi: 10.19487/j.cnki.1001-8425.2019.09.004
30. Zhang L, Sun G, Shen J, et al. Design and experimental study of acoustical enclosure for reactor (Chinese). Journal of Harbin Engineering University. 2007; 28(12): 1352–1355+1381.
31. Xu S. Design and analysis of interference noise reduction devices on low-height noise barriers near urban rail transit. Dissertation [Master's thesis] (Chinese). Chengdu: Southwest Jiaotong University; 2019.
32. Murata K, Nagakura K, Kitagawa T, et al. Noise reduction effect of noise barrier for Shinkansen based on Y-shaped structure. Quarterly Report of RTRI. 2006; 47(3): 162–168. doi: 10.2219/rtriqr.47.162
33. May DN, Osman NM. The performance of sound absorptive, reflective, and T-profile noise barriers in Toronto. Journal of Sound & Vibration. 1980; 71(1): 73–101. doi: 10.1016/0022-460X(80)90409-5
34. Yin H, Li Z, He C, et al. Interference noise reduction component for railway platforms. Patent CN105755973A, 28 April 2016.
35. Veloso M, Pereira M, Godinho L, et al. Insertion loss prediction of sonic crystal noise barriers covered by porous concrete using the Method of Fundamental Solutions. Applied Acoustics. 2023; 211: 109543. doi: 10.1016/j.apacoust.2023.109543
36. Qin M, Wang J, Deng Q, Cai J. Insert loss experiment and acoustic impedance theoretical study on the noise barrier with MPP-QRD top structure. Applied Acoustics. 2024; 221: 109996. doi: 10.1016/j.apacoust.2024.109996
37. Tarrazó-Serrano D, Castiñeira-Ibáñez S, San Bautista A, et al. Optimization of acoustic subwavelength slit barrier to control low-frequency noise in industrial buildings. Journal of Building Engineering. 2025; 103: 111926. doi: 10.1016/j.jobe.2025.111926
38. NSAI Standard. Electroacoustics - Sound level meters - Part 1: Specifications. NSAI Standard; 2013.
39. He B, Xiao X, Zhou X, et al. Numerical simulation of acoustic performance of geometric shapes of high-speed railway noise barriers. Journal of Mechanical Engineering. 2016; 52(2): 99–107.
40. Ge T, Gong Z, Wang ZZ. Derivation of the calculation formula for the sound pressure level radiated by a plane sound source of arbitrary shape (Chinese). Noise and Vibration Control. 1987; 02: 12–17.
41. Attenborough K. Ground parameter information for propagation modeling. Acoustical Society of America Journal. 1992; 92(5): 3007.
42. Du GH, Zhu ZM, Gong XF. Fundamentals of acoustics, 3rd edition (Chinese). Nanjing, China: Nanjing University press; 1981.